Acoustophoretic Contactless Elevation, Orbital Transport and Spinning of Matter in Air

Daniele Foresti and Dimos Poulikakos*
Department of Mechanical and Process Engineering, Laboratory of Thermodynamics in Emerging Technologies, Institute of Energy Technology, ETH Zurich, CH-8092 Zurich, Switzerland
(Received 4 March 2013; revised manuscript received 21 October 2013; published 15 January 2014)

We present the experimental demonstration and theoretical framework of an acoustophoretic concept enabling contactless, controlled orbital motion or spinning of droplets and particles in air. The orbital plane is parallel to gravity, requiring acoustophoretic lifting and elevation. The motion (spinning, smooth, or turnstile) is shown to have its origin in the spatiotemporal modulation of the acoustic field and the acoustic potential nodes. We describe the basic principle in terms of a superposition of harmonic acoustic potential sources and the intrinsic tendency of the particle to locate itself at the bottom of the total potential well.

DOI: 10.1103/PhysRevLett.112.024301 PACS numbers: 43.25.Uv, 47.11.Fg, 47.55.D-

Contactless positioning and transport of matter in air is scientifically and technically very challenging but carries with it significant potential benefits for a wide range of applications requiring high purity, low contamination, and negligible friction [1–4]. Additionally, basic research strongly benefits from contactless handling. Microgravity or zero-gravity experiments, for example, are often needed for accurate results [5,6], but their costs, usually connected to space flights or, for limited time experiments, to drop towers, can be prohibitive. Magnetic [7], electrical [8], and optical [9] forces are extensively exploited for such purposes, but are intrinsically material property dependent, possibly requiring laborious samples preparation [10].

In recent years, the involvement of acoustic radiation pressure [2] is experiencing a growing role in contactless handling, mostly driven by lab-on-chip applications, where the use of a liquid as acoustic medium accounts for a significant aiding and enabling buoyancy force [11]. When the host fluid is a gas [12,13,14,15], several critical issues need to be addressed and a deeper understanding of the related physics is necessary [16]. This includes the absence of appreciable buoyancy force, difficulties of sound transmission between source and the acoustic medium [17], evaporation, and breakup phenomena when dealing with droplet levitation [18,19]. In such context, near-field acoustic levitation has been shown to move contactlessly high density material such as glass or metal, but the technique is limited to flat, solid samples [20].

The fact that a sound wave could exert a torque dates back to more than a century ago [21]. Albeit a general theory has been proposed [22–25], experimental exploitation has been limited [26]. An advantageous method for rotation of microsized, nonspherical particles in an aqueous environment was recently reported by Dual *et al.* [27], where the amplitude modulation of the acoustic field was employed to orient multiple samples on a chip. An acoustic beam carrying orbital angular momentum has been used to apply a small torque to a suspended disk, but no levitation of the sample was involved [28]. To date, rotation of ultrasonically levitated glycerol droplets has been achieved by means of an acoustic torque [29]. This mechanism has the advantage of applying a torque to a symmetric object, but since the torque is based on viscous stresses [30,31], it is not controllable, nor useful for angular positioning: a residual rotation of the sample at a frequency ranging between 2 to 5 Hz is unavoidable.

The dynamics of a levitated particle in a simple geometry has been studied by Barrios and co-workers [32]. Although solving numerically the complete Navier-Stokes equationsin the time domain provides a thorough insight on the physics of the problem [33], it is also computationally very expensive and not practical for large domains, compared to other simplified modeling approaches such as the Gorkov potential [34,35], which can be in this respect of significant utility.

In this Letter, we present a novel concept of acoustic manipulation of matter in air, enabling controlled orbital transport and spinning. By determining and modulating the acoustic field evolution in a circular region generated by discrete, peripherally placed resonators, we were able to spin or set in circular orbit liquid droplets and solid particles in the mm range in air. The physical phenomenon and its dynamics are modeled and their nature explained with a one-dimensional analytical model, followed by a full three-dimensional numerical model for accurate quantification.

In acoustic levitation, an acoustic standing wave is established between an emitting surface and a reflector [2]. The radiation pressure, a nonlinear property of the acoustic field, engenders the Gorkov acoustic potential [34]. Despite some limitations on particle size and multiple scattering effects [36], this potential conveniently predicts the levitation sites of small spherical objects of radius R_s in an acoustic field generated by a standing wave. Employing the root mean square acoustic pressure p_{rms} and the velocity v_{rms} of the field, the Gorkov potential U is given by

$$\tilde{U} = 2\pi R_s^3 \left(\frac{p_{\mathrm{rms}}^2}{3\rho_0 c^2} - \frac{\rho_0 v_{\mathrm{rms}}^2}{2} \right), \quad (1)$$

where c and ρ_0 are the speed of sound and the density of the acoustic medium, respectively. The nondimensional form of the potential, $U = \tilde{U}/(2\pi R_s^3 \rho_0 V_0^2)$, is used here, where V_0 is the vibrational velocity amplitude of the emitter surface. The gradient of the potential predicts the acoustic force acting on the particle, $F_i = -\partial U/\partial x_i$. The particle experiences this acoustic force $\vec{F}$ and advances toward a potential well. At static conditions, if the acoustic force counterbalances the gravitational force, the levitated object is trapped at an equilibrium position.

The concept presented here is based on the spatiotemporal modulation of the acoustic potential nodes by varying their shape and size along concentric circular orbits, which can be used not only to obtain static levitation, but also to promote (1) spinning of an asymmetric sample at one predefined point and (2) an orbital motion in a plane parallel to gravity (denoted by g in Fig. 1). The resulting motion effectively demonstrates contactless acoustophoretic lifting of levitated matter in air.

Figure 1 and the Supplemental Material, Movie SM1 [41] show the experimental setup and proof of principle. The experimental setup is based on only three levitation elements (LEs) placed at 120° with respect to each other. Each LE is composed of an emitter and a reflector, placed at a distance $H \approx 5/2\,\lambda$, with λ being the acoustic wavelength (Fig. S1 [41]). This distance guarantees the formation of a standing wave with five levitation nodes along the vertical axis z.

The emitters of the LEs are driven such that controllable and selective emission of each LE is possible. During a spinning or revolution cycle of period T (rotation frequency $f_r = 1/T$), only two LEs are simultaneously operating. The emitter oscillates sinusoidally at ultrasonic frequency $f \approx 32.5$ kHz with a velocity amplitude V_0 proportional to the input voltage A_0. The voltage is modulated in a parabolic manner, as shown in Fig. 1. As a result, due to the quadratic nature of the acoustic radiation pressure [Eq. (1)], a nearly constant acoustic potential magnitude is obtained within the system during the node modulation process. The constancy of the acoustic potential is a key element when dealing with liquid samples in air and a distinguishing difference compared to solid particle handling: the acoustic force has to be strong enough to overcome the gravitational force, but still weaker than the surface tension force of the liquid, to avoid a breakup of the liquid [19,37,38]. This is achievable up to an upper limit of the levitated droplet radius R_s. For a water droplet levitated in air at $f = 32.5$ kHz the maximum radius is $R_s \approx 2.0$ mm [38].

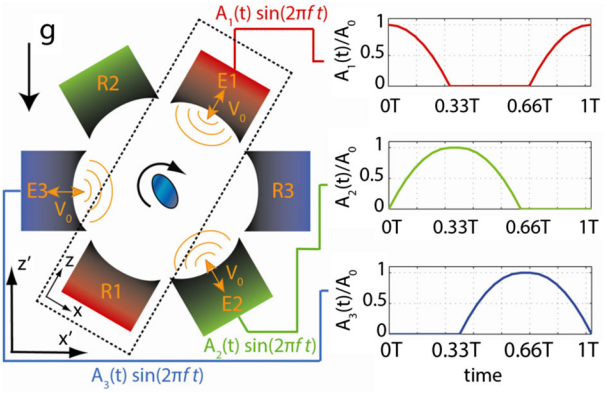

FIG. 1 (color online). Schematic of the handling system and its driving signal A_i (t). The x, y, and z axes represent the reference system relative to the LE, while the x', y', and z' axes represent the global reference system.

The proposed acoustic field modulation (Fig. 1) shapes the central node so that an asymmetric sample placed in it can experience torque. The acoustic nodes are generally ellipsoidal and they exert a stronger force on the vertical axis z (Fig. 1, [39]). When dealing with liquid samples, this potential distribution is responsible for the typical oblate droplet shape, balancing the acoustic forces with the surface tension forces [19]. In fact, the acoustic field stretches the droplets along the major axis due to the v_{rms} radiation pressure contribution [Eq. (1), [33]].

Three kinds of motion can simultaneously take place with levitated particles, as shown in Fig. 2(a) (Supplemental Material SM1, [41]). In orbit 0, at the center of the levitator, the acoustic field provides a torque and spins a nonspherical object [Fig. 2(b), see also Supplemental Material SM2 [41]]. This orbit is characterized by a strong and constant magnitude of the acoustic potential. A water droplet [$R_s \approx 0.5$ mm in

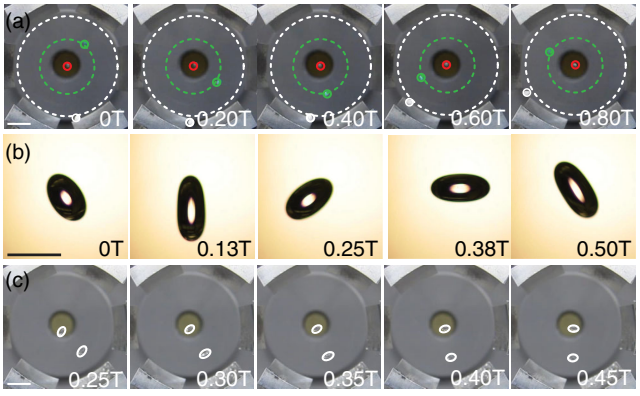

FIG. 2 (color online). (a) Orbit 0, at the center, red. Orbits 1 and 2 are denoted by green and white, respectively. The expanded polystyrene particles ($R_s \approx 0.6$ mm, $\rho_s = 0.04$ g/cm^3) are highlighted with a circle of the color of the corresponding orbit. (b) Water droplet spinning in orbit 0. The acoustic field distribution stretches the droplet to its typical ellipsoidal shape. (c) Two water droplets simultaneously handled. The droplet at orbit 0 rotates at its axis (spinning), while the droplet in orbit 1 is transported along a circular orbit. Scale bar: (a) 5, (b) 1, and (c) 5 mm.

Fig. 2(b)] can be levitated and spun during the entire emission period T, as a result of a controlled acoustic field exerting enough force to overcome the gravitational force without atomizing the droplet. The external orbits 1 and 2 can levitate and move a sample at the respective node, but they strongly differ in node-pattern movement and magnitude. In orbit 1, the potential is strong enough to levitate and transport a water droplet along $a \sim \pi/2$ rad part of the orbit [Fig. 2(c)], corresponding to about 10 mm of travel length. In addition, the transport of the sample is characterized by turnstile motion, with a sudden acceleration at three specific times, $0.22T, 0.55T$, and $0.88T$. On the other hand, the external orbit 2 exhibits a very smooth motion along the entire length of 64 mm, with a small departure from the circular path in correspondence with the gaps between the two successive LEs. Its rotational frequency is only one fourth of the rotation frequency f_r, and the acoustic field magnitude suffices for the levitation of only a light particle ($\rho_s = 0.04$ g/cm^3).

The Gor'kov potential requires the linear acoustic quantities p_{rms} and v_{rms} to determine the nonlinear acoustic forces [Eq. (1)]. Therefore, the acoustic wave equations in the frequency domain were solved by a three-dimensional FEM fluid-structure coupled model ([40], Supplemental Material [41].

The validated numerical model correctly captures the physics of the acoustophoretic concept and predicts well the experimental results. Figure 3(a) shows the potential nodes along with the experimental position of two manipulated expanded polystyrene spheres during the transition period T for both orbits 0 and 1. The good correspondence between acoustic potential node evolution in time and particle position is also evident for orbit 2, characterized by a weak potential (Supplemental Material SM1 [41]). To better quantify the comparison, the tracking of the particle coordinates of orbit 1 during a full revolution is presented in Figs. 3(b) and 3(c) for Cartesian (z', x') and radial (θ) coordinates, respectively. The motion discontinuities are captured well by the model that predicts the acoustic field evolution at $0.17T$, $0.5T$, and $0.83T$. At these specific times, the node splits into two subnodes, followed by a sudden change of particle position, when one node disappears at $0.22T$, $0.55T$, and $0.88T$. The travel between the first and the second subnode requires very low inertia for quick motion.

To better understand the physics of generating continuous motion from a discrete number of acoustic sources, we constructed an analytical model to calculate the acoustic potential evolution and to track its node minima positions

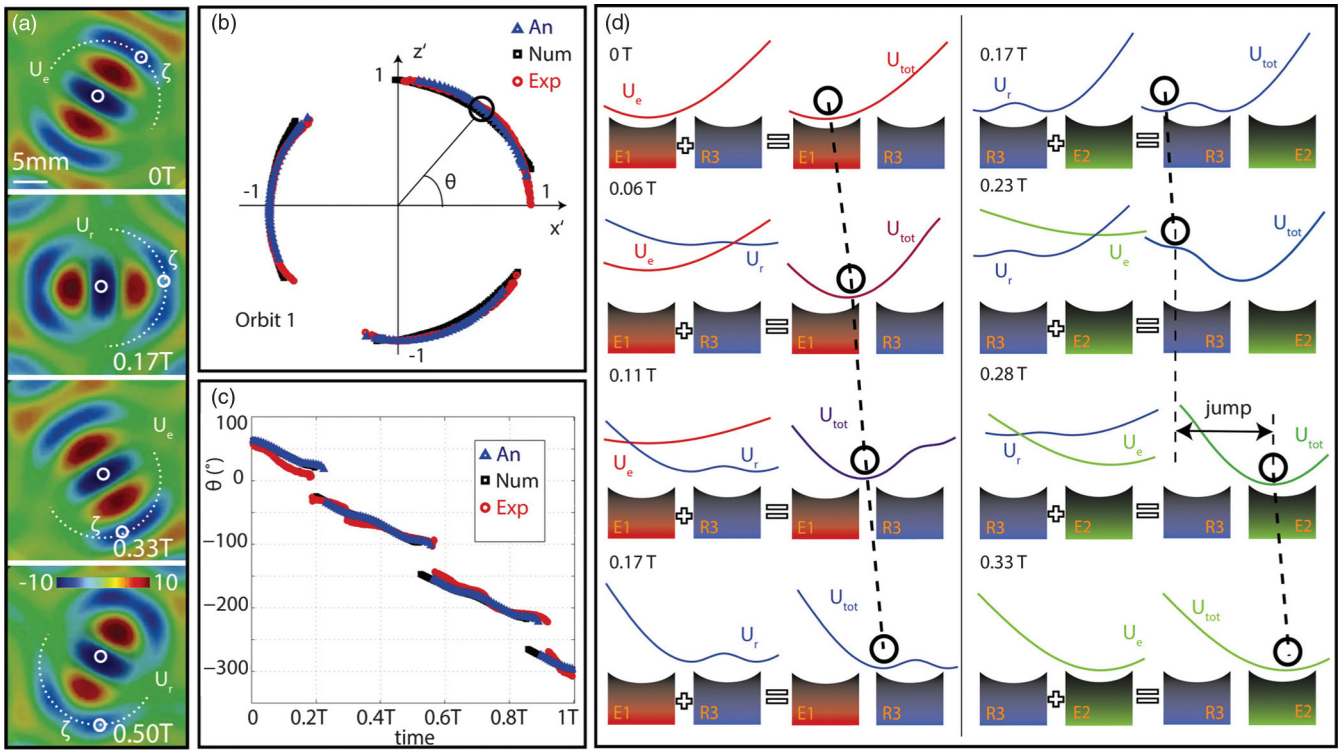

FIG. 3. (color) (a) Contour plot of the nondimensional Gorkov potential within the acoustophoretic manipulator. The white circles represent the two levitated particles during the experiment. (b) Cartesian (x', z', normalized values) and (c) radial (θ, degree) coordinates of the particle position predicted by the numerical and analytical models are plotted against the experimental data along orbit 1 $T = 26$ s). Movies were recorded with a digital camera and processed using the open source package ImageJ 1.46a. (d) Evolution of the acoustic potential between emitter—reflector—emitter. The continuous motion and the periodic discontinuities are explained by the acoustic potential pattern evolution, resembling a tilted washboard.

with respect to orbit 1. The acoustic potential U was treated as linear combination of six sources (three emitters, U_e, and three reflectors, U_r). If the acoustic field within the acoustic device at $0T$ and $0.17T$ [corresponding to U_r and U_e, respectively, Fig. 3(a)] is known, the full motion of a levitated particle can be predicted. The magnitudes of U_e and U_r are obtained from the numerical model: they are subsequently represented by a linear combination of cosine functions ([36], Supplemental Material [41]). Figure 3(a) and the Supplemental Material SM1 [41] highlight the fundamental difference between the two potentials: U_e is characterized by a single potential well, while U_r by two closely spaced such wells. This qualitative information is critical to understand the discontinuities and the turnstile nature of this orbit. By moving from an emitter to a reflector, the potential field $U_{\mathrm{tot}} = U_e + U_r$ allows a smooth transition because the particle is always located at the minimum of the total potential during its motion [Fig. 3(d), time 0–$0.17T$, movie SM2 in the Supplemental Material [41]]. The behavior strongly differs when moving from a reflector to an emitter. The particle is levitated on the left-hand side node until U_e overcomes U_r, smoothing out the left node and causing the particle to "jump" (motion discontinuity) toward the right-hand side node to reach the minimum of the total potential [Fig. 3(d), time 0.17–$0.33T$ movie SM2 in Supplemental Material [41]]. Such patterns repeat themselves for the following two motion segments, 0.33–$0.67T$ and 0.67–$1.0T$. The results of the analytical model show good agreement with the experiments [Figs. 3(b) and 3(c), Supplemental Material [41]].

The quasistatic models presented (numerical and analytical) are sufficient to track the levitated sample under the assumption of a "slow" motion of the particle compared to the acoustic force characteristic time (for a scaling analysis, see the Supplemental Material [41]). The concept is based on the temporal modulation of the acoustic potential: the levitated sample follows the node accordingly. On the other hand, this approach does not account for possible oscillations of the sample motion, visible during the experiments at the discontinuities. A more complete description of the physical phenomenon can be achieved by introducing the inertia and drag forces. For very light particles we can neglect the gravitational force (Supplemental Material [41]). The complete motion of the particle can be described as

$$m\ddot{\zeta} - k_d\dot{\zeta} + \phi_a(\zeta, t) = 0, \tag{2}$$

where ζ is the position along the orbit 1 of the sample, $m = 4/3\pi\rho_s {R_s}^3$ is its mass, k_d is the Stokes drag coefficient and $\phi_a(\zeta, t) = -\partial U_{\mathrm{tot}}(t)/\partial x_{O_1}|_{x_{O_1}=\zeta}$ is the acoustic force. For details about the dynamic model and its implementation in MATLAB, see the Supplemental Material [41].

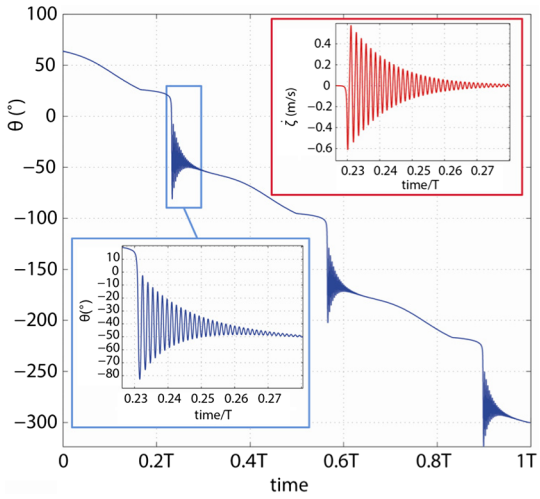

FIG. 4 (color online). Particle dynamics. The particle follows the acoustic node and shows strong oscillations at the discontinuities ($R_s = 0.6$ mm, $\rho_s = 0.04$ g/cm^3, $T = 26$ s, air viscosity $\mu = 20$ μPas, $V_0 = 1.45$ m/s).

The results are shown in Fig. 4. The particle position $\zeta(t)$ is expressed in the θ coordinate (in blue) during the entire revolution of period T. Despite some limitations of the measurements (the time resolution of the camera was of 25 fps $= 0.04$ s) and the experimental uncertainty of the acoustic field inside the levitator, a quantitative comparison is still possible. The oscillations after the discontinuity last for about 0.5 ± 0.1 s ($0.02 \pm 0.004\,T$), of the same order at the model prediction, 0.9 s ($0.035\,T$). Moreover, the model can predict the maximum linear velocity $\dot{\zeta}$ at the discontinuity (Fig. 4, red box). Its value of about 60 cm/s is greater than the maximum speed that could be measured (7 cm/s) due to the resolution limit of the camera, but is still low enough to justify the use of the Gor'kov potential (Supplemental Material [41].). Outside the discontinuity regions, $\dot{\zeta}$ depends on the period length T. In the experimental setup, T can be adjusted from infinite, corresponding to stable positioning, to 3.3 s, for a rotational frequency $f_r = 0.3$ Hz. The Supplemental Material, Movie SM3 [41] shows a water droplet rotating at 0.3 Hz at orbit 0. This rotational speed corresponds to an average linear speed of about 1.2 cm/s for orbit 1 (SM4, [41]).

A novel acoustophoretic orbital lifting concept was presented, demonstrated, and its physics explained theoretically. The concept enabled orbital motion in a plane parallel to gravity (requiring elevation) as well as spinning of matter. The spatiotemporal determination and control of the acoustic field made possible the orbiting and spinning of heavy matter, such as water droplets in the mm range, in air. A quasistatic theoretical model was developed to capture and predict the sample motion, and a one-dimensional model was developed to predict the sample dynamics. Possible applications range from the contactless material-independent handling of liquids and solids to substrate-independent biological reactions in drops.

Funding for this work provided by the Swiss National Science Foundation (SNF), Grant No. 144397 is gratefully acknowledged. We thank Paolo Francesco D'Aleo, ETH Zurich, for support with the electronics, Bruno Kramer, LTNT-ETH Zurich, for manufacturing of parts of the devices and Manish Tiwari, Carlo Antonini, and Thomas Vasileiou, LTNT-ETH Zurich, for the helpful discussions.

*To whom all correspondence should be addressed.
dpoulikakos@ethz.ch

[1] E. H. Brandt, Science **243**, 349 (1989).
[2] V. Vandaele, P. Lambert, and A. Delchambre, Precis. Eng. **29**, 491 (2005).
[3] R. Tuckermann, S. Bauerecker, and H. K. Cammenga, J. Colloid Interface Sci. **310**, 559 (2007).
[4] P. Aussillous and D. Quere, Nature (London) **411**, 924 (2001).
[5] R. E. Apfel *et al.*, Phys. Rev. Lett. **78**, 1912 (1997).
[6] T. G. Wang, E. H. Trinh, A. P. Croonquist, and D. D. Elleman, Phys. Rev. Lett. **56**, 452 (1986).
[7] R. J. A. Hill and L. Eaves, Phys. Rev. Lett. **101**, 234501 (2008).
[8] S. K. Chung and E. H. Trinh, J. Cryst. Growth **194**, 384 (1998).
[9] G. A. Swartzlander, T. J. Peterson, A. B. Artusio-Glimpse, and A. D. Raisanen, Nat. Photonics **5**, 48 (2011).
[10] J. R. Dorvee, A. M. Derfus, S. N. Bhatia, and M. J. Sailor, Nat. Mater. **3**, 896 (2004).
[11] H. Bruus, J. Dual, J. Hawkes, M. Hill, T. Laurell, J. Nilsson, S. Radel, S. Sadhal, and M. Wiklund, Lab Chip **11**, 3579 (2011).
[12] S. Baer, M. A. B. Andrade, C. Esen, J. C. Adamowski, G. Schweiger, and A. Ostendorf, Rev. Sci. Instrum. **82**, 105111 (2011).
[13] W. J. Xie, C. D. Cao, Y. J. Lü, and B. Wei, Phys. Rev. Lett. **89**, 104304 (2002).
[14] W. J. Xie and B. Wei, Phys. Rev. E **66** 026605 (2002).
[15] D. Koyama and K. Nakamura, IEEE Trans. Ultrason. Ferroelectr. Freq. Control **57**, 1152 (2010).
[16] D. Foresti, M. Nabavi, M. Klingauf, A. Ferrari, and D. Poulikakos, Proc. Natl. Acad. Sci. U.S.A. **110**, 12 549 (2013).
[17] F. Priego-Capote and L. de Castro, TrAC Trends in Analytical Chemistry **25**, 856 (2006).
[18] A. L. Yarin, G. Brenn, O. Kastner, D. Rensink, and C. Tropea, J. Fluid Mech. **399**, 151 (1999).
[19] C. P. Lee, A. V. Anilkumar, and T. G. Wang, Phys. Fluids **6**, 3554 (1994).
[20] S. Ueha, Y. Hashimoto, and Y. Koike, Ultrasonics **38**, 26 (2000).
[21] L. Rayleigh, Philos. Mag. XIV **186** (1882).
[22] G. Maidanik, J. Acoust. Soc. Am. **30**, 620 (1958).
[23] J. B. Keller, J. Acoust. Soc. Am. **29**, 1085 (1957).
[24] Z. Fan, D. Mei, K. Yang, and Z. Chen, J. Acoust. Soc. Am. **124**, 2727 (2008).
[25] G. T. Silva, T. P. Lobo, and F. G. Mitri, Europhys. Lett. **97**, 54003 (2012).
[26] S. Yamahira, S.-i. Hatanaka, M. Kuwabara, and S. Asai, Jpn. J. Appl. Phys. **39**, 3683 (2000).
[27] J. Dual, P. Hahn, I. Leibacher, D. Möller, T. Schwarz, and J. Wang, Lab Chip **12**, 4010 (2012).
[28] K. Volke-Sepulveda, A. O. Santillan, and R. R. Boullosa, Phys. Rev. Lett. **100**, (2008).
[29] A. Biswas, E. W. Leung, and E. H. Trinh, J. Acoust. Soc. Am. **90**, 1502 (1991).
[30] T. G. Wang, H. Kanber, and I. Rudnick, Phys. Rev. Lett. **38**, 128 (1977).
[31] F. H. Busse and T. G. Wang, J. Acoust. Soc. Am. **69**, 1634 (1981).
[32] G. Barrios and R. Rechtman, J. Fluid Mech. **596**, 191 (2008).
[33] D. Foresti, M. Nabavi, and D. Poulikakos, J. Fluid Mech. **709**, 581 (2012).
[34] L. P. Gorkov, Dokl. Akad. Nauk SSSR **140**, 88 (1961) [L. P. Gorkov, Soviet Phys.—Doklady **6**, 773 (1962)].
[35] S. L. Min, R. G. Holt, and R. E. Apfel, J. Acoust. Soc. Am. **91**, 3157 (1992).
[36] M. Barmatz and P. Collas, J. Acoust. Soc. Am. **77**, 928 (1985).
[37] D. Foresti, M. Nabavi, and D. Poulikakos, J. Acoust. Soc. Am. **131**, 1029 (2012).
[38] E. G. Lierke and L. Holitzner, Meas. Sci. Technol. **19**, 115803 (2008).
[39] W. J. Xie and B. Wei, Phys. Rev. E **70**, (2004).
[40] D. Foresti, N. Bjelobrk, M. Nabavi, and D. Poulikakos J. Appl. Phys. **109**, 093503 (2011).
[41] See Supplemental Material at http://link.aps.org/supplemental/10.1103/PhysRevLett.112.024301 for movies SM1-SM4 and details regarding 1. The levitation system 2. The quasi-static numerical model 3. The quasi-static analytical model 4. The validity limit of the quasi-static model 5. The dynamic model 6. Movie captions.